Maximum Efficiency Point Tracking in Inductive Links: Series versus Parallel Receiver's Compensation

Pablo Pérez-Nicoli and Fernando Silveira
Instituto de Ingeniería Eléctrica, Facultad de Ingeniería, Universidad de la República. Montevideo, Uruguay.
pablop@fing.edu.uy; silveira@fing.edu.uy

***Abstract*—The postregulation method of an inductive power link consists of adjusting its output voltage directly in the receiver by using a feedback dc-dc converter, thus without having to rely on back telemetry. In postregulated systems, the maximum efficiency point (MEP) of the link can be tracked by adjusting the transmitter voltage amplitude in closed-loop. In this paper, we analyze how the series and parallel receiver compensation affect differently the closed-loop control of the MEP tracking. The theoretical analysis proves that the MEP cannot be achieved with a series compensation but it can be attained with a parallel compensation. Additionally, the theoretical analysis predicts how any more complex resonant structure affects the attainability of the MEP. Finally, the analysis is validated by simulations and measurements. The proof-of-concept system postregulates the output voltage at 5 V and achieves the MEP of 40% in measurements while delivering 50 mW to the load, working at 13.56 MHz with 1-cm-air-gap and a 25mm$\times25$mm receiver.**

***Index Terms*—Inductive power transmission, maximum efficiency point, series compensation, parallel compensation.**

I. Introduction

Recently, Wireless Power Transfer (WPT) has shown to be a key factor for improving the robustness, usability, and autonomy of many mobile devices. The WPT link relaxes the trade-off between the battery size and the power availability, enabling highly innovative applications. Inductive Power Transfer (IPT) has been used in many works to transfer power in the centimeters range. The magnetic field causes less adverse effects on the human body than the electric field, thus IPT is the best choice for biomedical systems [1].

A block diagram of an IPT system is presented in Fig. 1. The system can be broadly divided into three blocks: the driver that powers the transmitter coil, the coupled coils (inductive link), and the receiver circuit that adapts the electromotive force to power the load. The total system efficiency, η_{TOT}, is the product of these three main blocks efficiencies, $\eta_{TOT} = \eta_{driver}.\eta_{link}.\eta_{RX}$.

Most of the loads require a regulated dc voltage. There are two main approaches to maintaining a constant voltage against coupling and load power variations which are known as preregulation and postregulation. In preregulation, the load voltage (V_L) is transmitted to the receiver in order to adjust the driver accordingly. In postregulation, the V_L is regulated directly in the receiver using a feedback dc-dc converter, thus without having to rely on back telemetry [2], [3]. In this paper, we address the Maximum Efficiency Point (MEP) tracking in postregulated systems.

It is well-known that it exists an optimum value for the input impedance of the receiver circuit (Z_{MN}, Fig. 1) which maximizes the link efficiency η_{link}. This optimum value is presented in (1), where L_{RX} and R_{RX} are the self-inductance and parasitic series resistance of the receiver coil respectively, $Q_{TX} = wL_{TX}/R_{TX}$ and $Q_{RX} = wL_{RX}/R_{RX}$ are the transmitter and receiver coil quality factors respectively, and k is the coupling coefficient between the coils.

$$Z_{MN_{opt}} = \underbrace{-jwL_{RX}}_{Im\{Z_{MN_{opt}}\}} + \underbrace{R_{RX}\sqrt{1+k^2Q_{TX}Q_{RX}}}_{Re\{Z_{MN_{opt}}\}} \quad (1)$$

The $Z_{MN_{opt}}$ depends on the coupling coefficient, and Z_{MN} is affected by the load power consumption (R_L, Fig. 1). Therefore, a dynamic adjustment is required to maintain $Z_{MN} = Z_{MN_{opt}}$ (MEP) against coupling and load variations.

In a postregulated system, the driver circuit can be adjusted to try to achieve and track $Z_{MN} = Z_{MN_{opt}}$ without requiring back telemetry, just minimizing the transmitted power, as is detailed later in Section II-B. However, it was reported [4]–[6] that if a series compensation is used in the receiver, the MEP cannot be directly achieved by minimizing the transmitted power.

In this work, we present a theoretical analysis that shows how the receiver compensation (series or parallel) affects differently the MEP attainability. Other more complex compensation structures have been proposed as the series-parallel presented in [7] and the matching network implemented in [8]. The analysis of this paper also predicts the effect of any resonant structure in the MEP attainability. This theoretical analysis is validated by simulations and measurements. The proof-of-concept system achieves the MEP of the link and postregulates the output voltage. In measurements, the MEP of 40% was achieved with a 1-cm-air-gap and a 25mm$\times25$mm receiver while regulating the output voltage to 5 V.

To the best of our knowledge, this is the first time that the effect of the receiver compensation (e.g. series or parallel) in the MEP tracking of postregulated system is analyzed.

This work was supported in part by the National Agency of Research and Innovation of Uruguay, FMV 3 2016 1 125877 and FMV 1 2017 1 136740

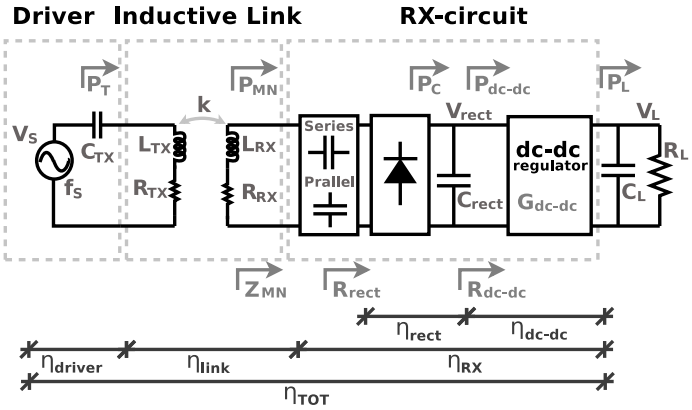

Fig. 1. Inductive power link block diagram. L_{TX} (L_{RX}) and R_{TX} (R_{RX}) are the self-inductance and parasitic series resistance of the transmitter (receiver) coil respectively. k is the coupling coefficient between coils. The transmitter resonance capacitor is $C_{TX} = 1/w^2 L_{TX}$. The blocks' efficiencies, intermediate powers, and input impedances are defined to be used in the theoretical analysis.

When the receiver compensation of a posregulated system is designed, the analysis of this paper should be considered to predict if the selected receiver compensation allows the system to achieve its MEP. In the cases where the MEP cannot be attained, a new design of the receiver compensation could be considered if it is possible, or other methods can be used as the transmitter k-impedance inverter proposed in [4].

This paper is organized as follows. First, Section II presents the theoretical analysis of the MEP tracking highlighting the differences between series and parallel compensation. In Section III, this analysis is validated by simulations and measurements of a proof-of-concept system. Finally, the main conclusions of this work are summarized in Section IV.

II. Theoretical Analysis

This analysis is divided into two subsections. First, in Section II-A, the operating point of the system is determined, highlighting the effect of the receiver compensation. Then, in Section II-B, the MEP tracking is explained showing that the series compensation is unable to achieve the MEP while the parallel compensation can attain that optimum point.

A. Operating point

To find the operating point of the system, the power balance in C_{rect} (Fig. 1) is analyzed. The system is working on a steady state when $P_C = P_{dc-dc}$ (Fig. 1). This steady state condition is presented in (2) as a function of the system parameters (Fig. 1), the transmitter and receiver coils quality factors, $Q_{RX\text{-}L}$ and Q_L which are defined in (3).

$$\underbrace{\overbrace{\frac{V_S^2}{2R_{TX}}\frac{k^2 Q_{TX} Q_{RX\text{-}L}}{(1+k^2 Q_{TX} Q_{RX\text{-}L})^2}\frac{Q_{RX\text{-}L}}{Q_L}}^{P_{MN}}\eta_{rect}}_{P_C} = \underbrace{\overbrace{\frac{V_L^2}{R_L}}^{P_L}\frac{1}{\eta_{dc\text{-}dc}}}_{P_{dc\text{-}dc}} \tag{2}$$

$$Q_L = \frac{wL_{RX}}{Re\{Z_{MN}\}} \; ; \; Q_{RX\text{-}L} = \frac{Q_{RX} Q_L}{Q_{RX} + Q_L} \tag{3}$$

TABLE I
Impedance transformation

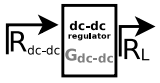	dc-dc regulator: $R_{dc\text{-}dc} = \eta_{dc\text{-}dc} R_L \overbrace{\left(\frac{V_{rect}}{V_L}\right)^2}^{\frac{1}{G_{dc\text{-}dc}}}$ (*) (4)
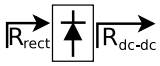	Rectifier: $R_{rect} = \frac{\eta_{rect} R_{dc\text{-}dc}}{2}$ (*) (5)
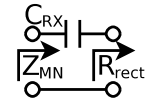	Series RX-MN: $Z_{MN} = \overbrace{R_{rect}}^{Re\{Z_{MN}\}} + \frac{1}{jwC_{RX}}$ (6)
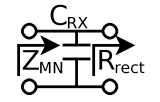	Parallel RX-MN: if $R_{rect}/(wL_{RX})^2 >> 1$ $Z_{MN} \simeq \overbrace{\frac{(wL_{RX})^2}{R_{rect}}}^{Re\{Z_{MN}\}} + \frac{1}{jwC_{RX}}$ (7)

(*) Deduced from power balance ($P_{in}.\eta = P_{out}$), neglecting parasitics capacitances, diodes threshold voltage and harmonic distortion.

The expression for P_{MN} in (2) can be deduced using reflected load theory [9], [10]. Then P_C and $P_{dc\text{-}dc}$ are deduced from the rectifier and dc-dc regulator efficiency definitions ($\eta_{rect} = P_C/P_{MN}$ and $\eta_{dc\text{-}dc} = P_L/P_{dc\text{-}dc}$).

From (2) it must be noted that all the parameters are predefined by the designer except for Q_L as explained next. This means that once the coils, the rectifier, the dc-dc regulator and the transmitter voltage are selected, the only parameter that could be adjusted to fulfill (2) is Q_L.

The Q_L depends on the real part of Z_{MN}, $Re\{Z_{MN}\}$, (3). Additionally, the $Re\{Z_{MN}\}$ is affected by the subsequent blocks of the receiver, the impedance transformations of all the blocks in the receiver are presented in Table I.

From Table I, it can be seen that there is a correspondence between the output voltage of the rectifier, V_{rect}, and the value of $Re\{Z_{MN}\}$. Therefore, the system achieves the steady state, when V_{rect} achieves the value that sets the $Re\{Z_{MN}\}$ that verifies (2). In the system presented in Fig. 1, at start-up $V_{rect} = 0$, and this voltage will increase until (2) is fulfilled.

In Fig. 2, the left side of equality (2) (P_C), and the right side of it ($P_{dc\text{-}dc}$) are represented as a function of the real part of Z_{MN}, $Re\{Z_{MN}\}$. Based on (2), it can be verified that $P_{dc\text{-}dc}$ is independent of $Re\{Z_{MN}\}$, and P_C has the shape represented in Fig. 2, regardless of the parameters values. As can be seen from Fig. 2, if $P_{dc\text{-}dc}$ is too high ($P_{dc\text{-}dc} > P_{C_{MAX}}$), there is no $Re\{Z_{MN}\}$ that satisfies (2). In that situation, the system is not going to work, because the receiver is demanding more power than the one available. On the other hand, if $P_{dc\text{-}dc} < P_{C_{MAX}}$, two values of $Re\{Z_{MN}\}$ that satisfy (2) exist, $Re\{Z_{MN}\}_L$ and $Re\{Z_{MN}\}_R$. One of these values is stable while the other is unstable, depending on the receiver compensation, as is detailed below.

To determine which of the two is the operating point, we analyze the system response to a perturbation in V_{rect}, with a parallel and series compensation. First, in (8) this analysis is presented for the case of $Re\{Z_{MN}\} = Re\{Z_{MN}\}_L$ (see Fig. 2) with a parallel compensation. Note that in each step

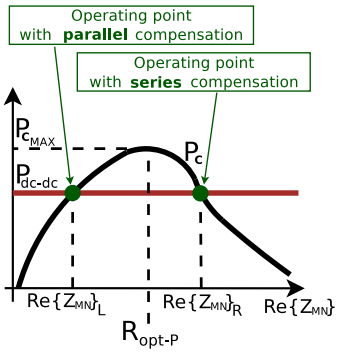

Fig. 2. Operating point (2) representation.

$Re\{Z_{MN}\}_L$ with parallel compensation

$$V_{rect} \uparrow \overset{(4)}{\Longrightarrow} R_{dc-dc} \uparrow \overset{(5)}{\Longrightarrow} R_{rect} \uparrow \overset{(7)}{\Longrightarrow} Re\{Z_{MN}\} \downarrow \overset{Fig.2}{\Longrightarrow} P_C < P_{dc-dc} \overset{Fig.1}{\Longrightarrow} V_{rect} \downarrow \quad (8)$$

$Re\{Z_{MN}\}_R$ with series compensation

$$V_{rect} \uparrow \overset{(4)}{\Longrightarrow} R_{dc-dc} \uparrow \overset{(5)}{\Longrightarrow} R_{rect} \uparrow \overset{(6)}{\Longrightarrow} Re\{Z_{MN}\} \uparrow \overset{Fig.2}{\Longrightarrow} P_C < P_{dc-dc} \overset{Fig.1}{\Longrightarrow} V_{rect} \downarrow \quad (9)$$

the number of the equation or figure used is indicated. The up arrow (↑) and down arrow (↓) indicate an increase or decrease in the variable value respectively. Equation (8) shows that $Re\{Z_{MN}\} = Re\{Z_{MN}\}_L$ with the parallel resonator is stable. The case for $Re\{Z_{MN}\} = Re\{Z_{MN}\}_R$ with the parallel resonator is not presented but can be deduced from (8) noting that the only different step is the one that depends on Fig. 2. In that case, a decrease in $Re\{Z_{MN}\}$ (from $Re\{Z_{MN}\}_R$) generates that $P_C > P_{dc-dc}$ thus increasing V_{rect}. Therefore, $Re\{Z_{MN}\} = Re\{Z_{MN}\}_R$ ends up being unstable when using a parallel resonator.

The series resonator is analyzed in (9) for the case of $Re\{Z_{MN}\} = Re\{Z_{MN}\}_R$. As can be seen from (6) and (7), the relationship between $Re\{Z_{MN}\}$ and R_{rect} is direct for (6) and inverse for (7). This difference between series and parallel resonator generates that the point ($Re\{Z_{MN}\}_L$ or $Re\{Z_{MN}\}_R$) that was stable with a parallel resonator, became unstable with a series resonator and vice versa. Therefore, the $Re\{Z_{MN}\}_R$ that was shown to be unstable with the parallel resonator, is stable with the series resonator (9). The unstable case of $Re\{Z_{MN}\}_L$ with a series resonator is not presented but it can be deduced from (9) noting that in this case when $Re\{Z_{MN}\} \uparrow$ (from $Re\{Z_{MN}\}_L$) $\Rightarrow P_C > P_{dc-dc}$ (Fig. 2), inverting the final result.

Although this analysis was done for the parallel and series compensation, it can be easily generalized for any general resonant topology. It can be noted that the only relevant information to determine the operating point was the relationship between the input impedance of the resonant structure and its load impedance. On the one hand, if this relationship is direct ($R_{rect} \uparrow\Rightarrow Re\{Z_{MN}\} \uparrow$) as in the series compensation case, the operating point is the one on the right (Fig. 2). On the other hand, if this relationship is inverse ($R_{rect} \uparrow\Rightarrow Re\{Z_{MN}\} \downarrow$) as in the parallel compensation case, the operating point is the one on the left (Fig. 2).

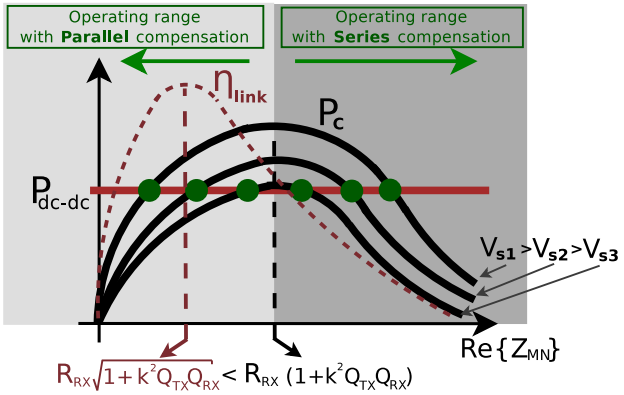

Fig. 3. System operating range versus transmitter voltage (V_S) for parallel and series compensation.

B. MEP tracking

In the previous section, the operating point was analyzed highlighting the difference between series and parallel compensation, Fig. 2. In this section, it is analyzed how this operating point can be modified to achieve the MEP.

As discussed in Section I, an optimum value for $Re\{Z_{MN}\}$ exists that maximizes the link efficiency (1). In order to achieve this optimum value, the P_C curve represented in Fig. 2 can be moved by changing the transmitter voltage V_S (Fig. 1), modifying the operating point. The P_C is proportional to V_S^2 (2), thus a variation in V_S only scales the curve of P_C as is represented in Fig. 3. Therefore, the possible ranges of $Re\{Z_{MN}\}$ with a parallel and a series compensation are represented in Fig. 3.

The link efficiency is also represented in Fig. 3. The $Re\{Z_{MN}\}$ that maximizes the link efficiency is lower than the one that maximizes P_C. Therefore, the MEP is within the operating zone that can be achieved with a parallel compensation, and is not included in the series region.

Summarizing the theoretical analysis, if a parallel compensation is used (or any compensation that inverts the impedance, $R_{rect} \uparrow\Rightarrow Re\{Z_{MN}\} \downarrow$) the MEP can be achieved by modifying the transmitter voltage. However, when a series compensation is used (or any compensation that does not invert the impedance, $R_{rect} \uparrow\Rightarrow Re\{Z_{MN}\} \uparrow$) it is not possible to reach the MEP just by changing the transmitter voltage.

In previous work such as [4], a k-impedance inverter in the transmitter is used to modify the P_C curve. The k-impedance inverter modifies the value of the $Re\{Z_{MN}\}$ that maximizes P_C thus changing the operating range achieved by each compensation, and allowing the system to achieve the MEP even with a series resonator.

To the best of our knowledge, this is the first time that the effect of the receiver compensation topology in the MEP tracking of postregulated systems is analyzed. In the next section, the analysis is validated by numerical calculation, circuit simulation, and measurement results of a proof-of-concept system.

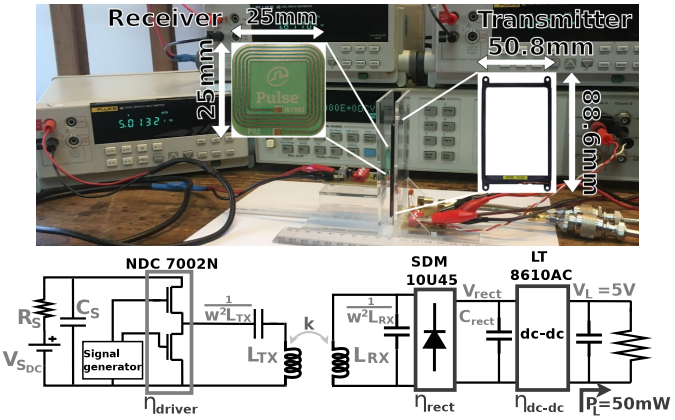

Fig. 4. Measurement setup and schematic of the proof-of-concept system.

TABLE II
PROOF-OF-CONCEPT PARAMETERS VALUES

$L_{TX} = 1.18$ μH ; $Q_{TX} = wL_{TX}/R_{TX} = 146.5$ (Pulse Elec. W7002)
$L_{RX} = 877$ nH ; $Q_{RX} = wL_{RX}/R_{RX} = 34.1$ (Pulse Elec. W7001)
$k = 0.08$ ($D = 1$ cm) ; $f_T = 13.56$ MHz ; $P_L = 50$ mW ; $V_L = 5$ V
$\eta_{driver} \simeq 90\%$; $\eta_{rect} \simeq 90\%$; $\eta_{dc\text{-}dc} \simeq 75\%$

III. Simulation and Measurement Results

The proof-of-concept system of Fig. 4, whose characteristics are presented in Table II, was simulated and measured.

The numerical calculation and simulation results are presented in Fig. 5. In the simulation, a rectifier with ideal diodes ($V\gamma = 0$) and an ideal dc-dc converter were used. The power load was set to $P_L/(\eta_{rect}.\eta_{dc\text{-}dc})$ to include these losses. The dc-dc regulator was turned ON after V_{rect} has been stabilized, to allow start-up. The $Re\{Z_{MN}\}$ obtained with parallel and series compensation in simulations are represented with a cross mark in Fig. 5. It can be seen that each point corresponds to the left and right operating points analyzed in Section II, thus validating the analysis.

In measurements, the total system efficiency was obtained measuring the power delivered by the dc voltage source $V_{S_{DC}}$ using the shunt resistor R_S (Fig. 4), and the power received by the load V_L^2/R_L. The measured efficiency, as a function of the $V_{S_{DC}}$, is presented in Fig. 6.

As was predicted by the model, the system with parallel compensation is able to reach the MEP ($\simeq$ 40%), just changing the transmitter voltage. The point with the lowest $V_{S_{DC}}$ measured in Fig. 6 corresponds to the case where $P_{C_{MAX}} = P_{dc\text{-}dc}$, see Fig. 2.

IV. Conclusion

The influence of the receiver compensation topology on the MEP tracking of postregulated systems was analyzed. The theoretical analysis allows the reader to predict the attainability of the MEP with series, parallel or any more complex compensation structure. The analysis was validated comparing numerical calculation, circuit simulation, and measurement results. In a proof-of-concept system with a 1-cm-air-gap and a 25mm×25mm receiver, the MEP of 40% was achieved just by adjusting the transmitter voltage.

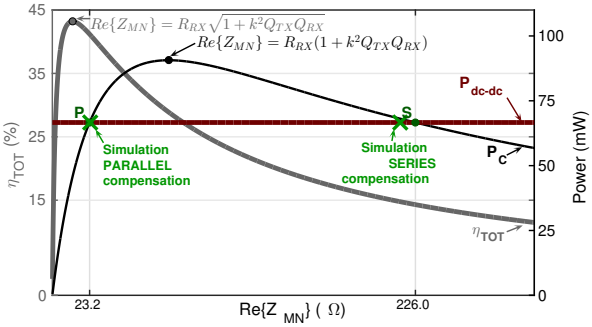

Fig. 5. Numerical calculation and simulation results using the values presented in Table II.

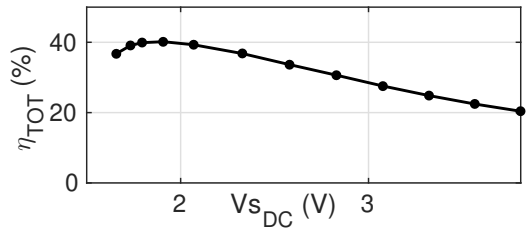

Fig. 6. Total system efficiency, η_{TOT}, from dc source to dc load, as a function of $V_{S_{DC}}$.

References

[1] T. Sun, X. Xie, and Z. Wang, *Wireless power transfer for medical microsystems*. Springer, 2013.

[2] H. Li, J. Li, K. Wang, W. Chen, and X. Yang, "A maximum efficiency point tracking control scheme for wireless power transfer systems using magnetic resonant coupling," *IEEE Transactions on Power Electronics*, vol. 30, no. 7, pp. 3998–4008, July 2015.

[3] W. X. Zhong and S. Y. R. Hui, "Maximum energy efficiency tracking for wireless power transfer systems," *IEEE Transactions on Power Electronics*, vol. 30, no. 7, pp. 4025–4034, July 2015.

[4] Y. Narusue, Y. Kawahara, and T. Asami, "Maximizing the efficiency of wireless power transfer with a receiver-side switching voltage regulator," *Wireless Power Transfer*, vol. 4, no. 1, pp. 42–54, 2017.

[5] S. Chen, H. Li, and Y. Tang, "A monotonic output regulation method for series-series compensated inductive power transfer systems with improved efficiency and communication-less control," in *2018 IEEE Energy Conversion Congress and Exposition (ECCE)*, Sep. 2018, pp. 6173–6178.

[6] H. Li, Y. Tang, K. Wang, and X. Yang, "Analysis and control of post regulation of wireless power transfer systems," in *2016 IEEE 2nd Annual Southern Power Electronics Conference (SPEC)*, Dec 2016, pp. 1–5.

[7] L. Chen, S. Liu, Y. C. Zhou, and T. J. Cui, "An optimizable circuit structure for high-efficiency wireless power transfer," *IEEE Transactions on Industrial Electronics*, vol. 60, no. 1, pp. 339–349, Jan 2013.

[8] R. Xue, K. Cheng, and M. Je, "High-efficiency wireless power transfer for biomedical implants by optimal resonant load transformation," *IEEE Transactions on Circuits and Systems I: Regular Papers*, vol. 60, no. 4, pp. 867–874, April 2013.

[9] M. Kiani, U. Jow, and M. Ghovanloo, "Design and optimization of a 3-coil inductive link for efficient wireless power transmission," *IEEE Transactions on Biomedical Circuits and Systems*, vol. 5, no. 6, pp. 579–591, Dec.

[10] P. Pérez-Nicoli and F. Silveira, "Maximum efficiency tracking in inductive power transmission using both matching networks and adjustable ACDC converters," *IEEE Transactions on Microwave Theory and Techniques*, vol. 66, no. 7, pp. 3452–3462, July 2018.